Massive spatial qubits: Testing macroscopic nonclassicality and Casimir entanglement

Bin Yi ®,[1] Urbasi Sinha,[2] Dipankar Home,[3] Anupam Mazumdar,[4] and Sougato Bose ®[1]

[1]*Department of Physics and Astronomy, University College London, Gower Street, WC1E 6BT London, United Kingdom*
[2]*Raman Research Institute, C. V. Raman Avenue, Sadashivanagar, Bengaluru, Karnataka 560080, India*
[3]*Center for Astroparticle Physics and Space Science (CAPSS), Bose Institute, Kolkata 700 091, India*
[4]*Van Swinderen Institute, University of Groningen, 9747 AG Groningen, Netherlands*

An open challenge in physics is to expand the frontiers of the validity of quantum mechanics by evidencing nonclassicality of the center of mass state of a macroscopic object. Yet another equally important task is to evidence the essential nonclassicality of the interactions which act between macroscopic objects. Here we introduce a new tool to meet these challenges: massive spatial qubits. In particular, we show that if two distinct localized states of a mass are used as the $|0\rangle$ and $|1\rangle$ states of a qubit, then we can measure this encoded spatial qubit with a high fidelity in the σ_x, σ_y, and σ_z bases simply by measuring its position after different duration of free evolution. This technique can be used reveal the irreducible nonclassicality of the spin and center of mass entangled state of a nanocrystal implying macrocontextuality. Further, in the context of Casimir interaction, this offers a powerful method to create and certify non-Gaussian entanglement between two neutral nano-objects. The entanglement such produced provides an empirical demonstration of the Casimir interaction being inherently quantum.

I. INTRODUCTION

It is an open challenge to witness a nonclassicality in the behavior of the center of mass of a massive object [1,2]. While there are ideas to observe nonclassicalities of ever more massive objects [3–13], the state-of-the-art demonstrations have only reached up to macromolecules of 10^4 amu mass [14,15]. Such demonstrations would test the limits of quantum mechanics [16–21], would be a stepping stone to witness the quantum character of gravity [22–26], and would open up unprecedented sensing opportunities [27]. Identifying new tools to probe macroscopic nonclassicality (by which here we mean in terms of large mass) is thus particularly important. Here we propose and examine the efficacy of precisely such a tool: a mechanism to read out a qubit encoded in the spatial degree of freedom of a *free (untrapped) mass* (a purely spatial qubit). A principal merit of this scheme is that *measuring the spatial qubit operators* σ_x, σ_y, and σ_z exploits solely the free time evolution of the mass (Hamiltonian $H = \hat{p}^2/2m$), followed by the detection of its position. As the mass is not controlled/trapped by any fields during its free evolution, decoherence is minimized.

As a first application, we show that our tool enables the verification of an irreducible nonclassicality of a particular joint state of a spin (a well established quantum degree spin) and the center of mass of a macroscopic object, whose quan-

tum nature is yet to be established. To this end, we use the state produced in a Stern-Gerlach apparatus which is usually written down as an *entangled* state of a spin and the position [25,28–32]. Such Stern-Gerlach states have been created with atoms with its spatial coherence verified after selecting a specific spin state [31,33]. However, there are, as yet, no protocols to verify the *entanglement* between the spin of an object in a Stern-Gerlach experiment and the motion of its center of mass in a way which can be scaled to macroscopic objects. We show that this can be accomplished via the violation of a Bell's inequality in which the spin and the positions of the mass are measured. This violation will also prove the nonclassicality of a large mass in terms of quantum contextuality [34,35].

Next, we propose a second application once the quantum nature of the center of mass degree of freedom of macroscopic objects is assumed (or established in the above, or in some other way). This application has import in establishing the quantum nature of the *interactions* between macroscopic objects. We show how our spatial qubit methodology can enable witnessing the entanglement created between two neutral nanocrystals through their Casimir interaction. This has two implications: (a) It will empirically show that the extensively measured Casimir interaction [36–38] is indeed quantum (e.g., is mediated by virtual photons similar to [39,40]—if photons are replaced by classical entities they would not entangle the masses [22–24,41,42]). (b) As the entangled state is generated by starting from a superposition of localized states, it is non-Gaussian. While there are ample methods for generating [43–45] and testing [46] Gaussian entanglement of nanocrystals, there is hardly any work on their non-Gaussian counterparts.
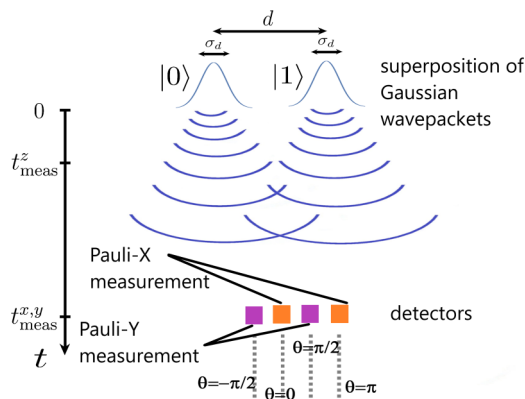
FIG. 1. Spatial detection for σ_x, σ_y measurements: a pair of detectors (color: orange) located at phase angle $\theta = 0$, $\theta = \pi$ perform σ_x measurement. The detectors (color: purple) at $\theta = \pi/2$, $\theta = -\pi/2$ perform σ_y measurement.

We are achieving our tool by combining ideas from two different quantum technologies: photonic quantum information processing and the trapping and cooling of nanocrystals. In the former field a qubit can be encoded in the spatial mode of a single photon by passing it through an effective Young's double slit [47]. These qubits, called Young qubits, and their d-level counterparts [48,49], have been exploited in quantum information [50,51]. On the other hand, we have had a rapid development recently in the field of levitated quantum nano-objects [7,8,52] culminating in their ground-state cooling and the verification of energy quantization [53,54]. While several schemes for verifying quantum superposition of distinct states of such objects have been proposed to date, in these schemes, either the x, y, and z motions are measured as infinite dimensional systems [10,55,56] rather than being discretized as an effective qubit, or never measured at all (only ancillary systems coupled to them are measured [11,12]). Here we adapt the idea of Young qubits from photonic technologies to massive systems. Note that a very different encoding of a qubit in the continuous variables of a harmonic oscillator was proposed long ago for quantum error correction [57], which is not suited to an untrapped nanocrystal.

II. QUBIT ENCODING AND ITS MEASUREMENT IN ALL BASES

Our encoding is intuitive: $|0\rangle$ and $|1\rangle$ states of a qubit are represented by two spatially separated (say, in the x direction) nonoverlapping wavepackets whose position and momenta are both centered around zero in the other two commuting (y and z) directions. Explicitly, these states (writing only the x part of their wavefunction) are

$$|0\rangle = \frac{1}{\sqrt{\sigma_d}\pi^{1/4}} \int_{-\infty}^{\infty} \exp\left[-\frac{(x + d/2)^2}{4\sigma_d^2}\right] |x\rangle dx, \quad (1)$$

$$|1\rangle = \frac{1}{\sqrt{\sigma_d}\pi^{1/4}} \int_{-\infty}^{\infty} \exp\left[-\frac{(x - d/2)^2}{4\sigma_d^2}\right] |x\rangle dx, \quad (2)$$

with $d \gg \sigma_d$. These states are schematically depicted in Fig. 1 in which only the x direction is depicted along with their

evolution in *time*. For simplicity, we will omit the acceleration due to the Earth's gravity (as if the experiment is taking place in a freely falling frame), which can easily be incorporated as its effect commutes with the rest. Thus we only consider one-dimensional (1D) time evolution in the x direction. In this paper, we will only require two states: (a) a state in which a spin embedded in a mass is entangled with the mass's spatial degree of freedom in the state $|\phi^+\rangle = \frac{1}{\sqrt{2}}(|\uparrow, 1\rangle + |\downarrow, 0\rangle)$ for our first application, and (b) the spatial qubit state $|+\rangle = \frac{1}{\sqrt{2}}(|0\rangle + |1\rangle)$ as a resource for our second application. Preparation of the above adapts previous proposals and will be discussed with the respective applications.

We now outline our central tool: the method of measuring the above encoded spatial qubit in various bases. The spatial detection can be performed by shining laser light onto the test masses [58,59]. The Rayleigh scattered light field acquires a position-dependent phase shift. The scheme is limited only by the standard quantum limit [58] (quantum back action) of phase measurement when a *large number of photons* are scattered from the mass. The resolution scales with the number n of scattered and detected photons as $\lambda/\sqrt{n}$, hence the power collected at the detector (see Eq. (13) of Ref. [59]), and the detection time (as long as this is lower than the dynamical time scale, it is independent of whether the particle is trapped/untrapped). Thus the detection time should be as much as one needs for the required resolution, but much less than the time span of the experiment. For the protocols we will present in this paper, we will base our calculations on a $\sim$60 nm diameter diamond nanoparticle (about $m \sim 10^{-19}$ kg mass). By the above methodology, for a 60 nm diameter particle, the detection resolution can reach 200 ± 20 fm/$\sqrt{\text{Hz}}$ with laser power $\sim$385 μW at the detector, at environmental pressure $\sim$0.01 mbar [59]. Thus for an integration time of $\delta t_{\text{int}} \sim 4$ μs, the resolution reaches $\sim$1 Å, which corresponds to just $\sim 10^8$ photons. Moreover, we are measuring this mass as a free particle, with an initial position spread. So the standard quantum limit of position measurement here (for a free particle) is [60] $\sim \sqrt{\frac{\hbar \delta t_{\text{int}}}{m}} \sim 2/3$ Å. Thus the measurement precision required is of the same order as the standard quantum limit (one does not need to go beyond it). As the whole measurement is μs, any noise of frequency lower than MHz will not affect it (simply remains constant during each measurement run). Moreover, lower frequency noise causing variation between, say, groups of runs, could be measured efficiently by other proximal sensors and taken into account. Also note that the spatial detection is performed at the very end of the protocol, so the question of back action on further position measurements does not arise.

Due to the spreading of the wavepackets along y and z directions, when we determine whether the object is in a given position $x = x_0$ at some measurement time t, we are essentially integrating the probability of detecting it over a finite region $\Delta y(t)$ and $\Delta z(t)$. The operator $\sigma_z = |0\rangle\langle 0| - |1\rangle\langle 1|$ is trivial to measure, as we simply shine a laser centered at $x = d/2$ much before the wavepacket states $|0\rangle$ and $|1\rangle$ have started to overlap [at a time $t^z_{\text{meas}} \ll d(2\sigma_d m)/\hbar$; the error in σ_z measurement as a function of t^z_{meas} is described in the Appendix A; timing errors $\delta t \ll t^z_{\text{meas}}$ have very little effect]. As described in the previous paragraph, if $\sim 10^8$ photons are
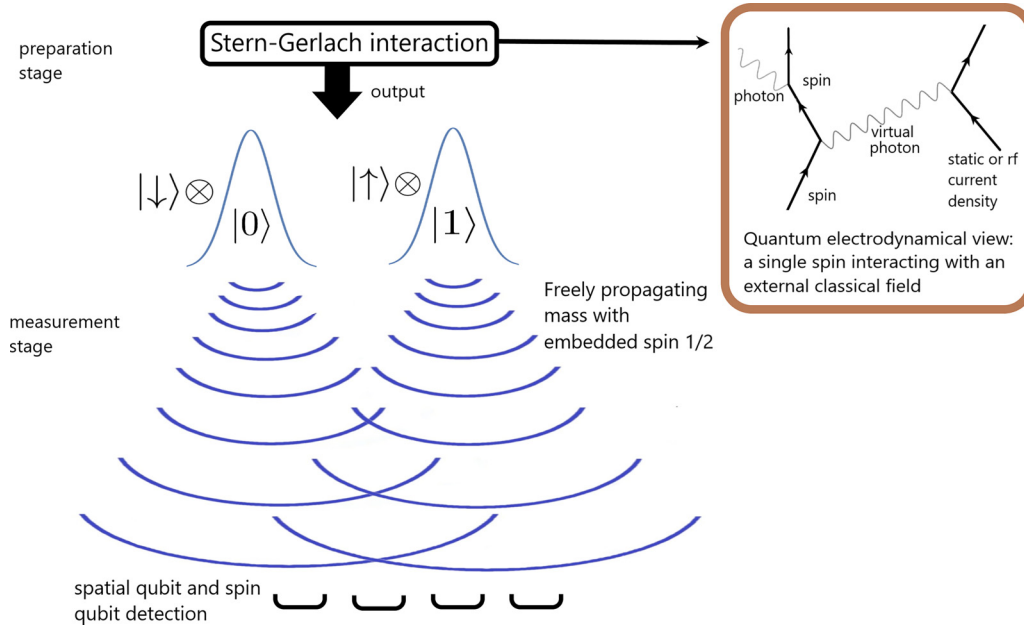
FIG. 2. Detection scheme for the entanglement of spin and center of mass of a Stern-Gerlach state: A spin bearing nano-object is measured to be in a set of zones of size δx, where the size is set by the strength and duration of lasers scattered from the object, which serves to measure the spatial qubit. Within each spatial zone a suitable method is used to measure the spin in different bases, for example, by rotating the spin states by microwave pulses followed by fluorescence of certain states under excitation by a laser of appropriate frequency.

scattered and collected, we can tell apart two states $|0\rangle$ and $|1\rangle$ separated by ~ 1 Å.

To measure the spatial qubit σ_x and σ_y operators, we need a large enough time $t_{\text{meas}}^{x,y} \geqslant d(2\sigma_d m)/\hbar$ so that the wavepackets of the $|0\rangle$ and $|1\rangle$ states have spread out enough to significantly overlap with each other and produce an interference pattern. Moreover, due to the free propagation, we would expect the measurement time $t_{\text{meas}}^{x,y}$, final position x, and the transverse wave vector k_x are related by $x = \frac{\hbar k_x t_{\text{meas}}^{x,y}}{m}$ (detecting at a position x after the interference effectively measures the initial superposition state of $|0\rangle$ and $|1\rangle$ in the $|k_x\rangle$ basis). Noting the momentum representation of the qubit states $|n\rangle = \int \{\sqrt{2}\sigma_d \exp[\frac{ik_x d}{2} - k_x^2 \sigma_d^2] \exp[-ink_x d]|k_x\rangle\} dk_x$ ($n = 0, 1$), the probability to detect the object at a position x for any initial qubit state $|\psi\rangle$ is given by

$$P(x) = |\langle\psi|k_x\rangle|^2 \propto \left| \exp\left[\frac{ik_x d}{2} - k_x^2 \sigma_d^2\right] \langle\theta|\psi\rangle \right|^2, \quad (3)$$

where $|\theta\rangle = |0\rangle + |1\rangle e^{i\theta}$ in which the parameter $\theta = k_x d = \frac{xmd}{\hbar t_{\text{meas}}^{x,y}}$ (we will call θ the phase angle). Therefore, finding the object in various positions x is in one to one correspondence with positive operator valued measurements (POVM) on the spatial qubit, with the relevant projection on the state being, up to a normalization factor, as $|\theta\rangle\langle\theta|$. σ_x measurements can therefore be implemented by placing a pair of position detectors (which will in practice be lasers scattering from the object) at positions corresponding to phase angle $\theta = 0, \theta = \pi$; Similarly, σ_y measurements can be achieved by placing detectors at $\theta = \pi/2, \theta = -\pi/2$ (Schematic shown in Fig. 1). For minimizing the time of the experiment, we are going to choose $t_{\text{meas}}^{x,y} = d(2\sigma_d m)/\hbar$. The efficacy of the σ_x and σ_y

measurements as a function of the finite time $t_{\text{meas}}^{x,y}$ for various ratios $\sigma_d : d$ is discussed in the Appendix.

III. NONCLASSICALITY OF THE STERN-GERLACH STATE

As a first application of this spatial qubit technology, we consider an extra spin degree of freedom embedded in a mesoscopic mass. We now imagine that the mass goes through a Stern-Gerlach apparatus. The motion of the mass relative to the source of the inhomogeneous magnetic field (current/magnets) is affected in a spin-dependent manner due to the exchange of virtual photons between the source and the spin (Fig. 2) resulting in an entangled state of the spin and position of the nano-object as given by $|\phi^+\rangle = \frac{1}{\sqrt{2}}(|\uparrow, 1\rangle + |\downarrow, 0\rangle)$, as depicted as the output of the preparation stage in Fig. 2. It could also be regarded as an intraparticle entanglement (an entanglement between two degrees of freedom of the same object), which has been a subject of several investigations [34,61,62].

To measure the spin-motion entanglement in $|\phi^+\rangle$, we have to measure variables of spin and spatial qubit. Here we specifically want to estimate the action of measuring one of these qubits on the quantum state of the other. During this measurement, the inhomogeneous magnetic field causing the Stern-Gerlach splitting is simply switched off so that spin coherence can be maintained using any dynamical decoupling schemes as required [63]. Alternatively, one can also use a more pristine nanodiamond with less surface defects. As shown in Fig. 2, after a required period of free evolution $t_{\text{meas}}^{x,y}$, measurements of the spatial qubit operators are made; the light shone on the object should not interact at all with the embedded spin degree of freedom if it is completely *off-resonant* with any relevant spin transition. Immediately

after measuring the spatial qubit, the spin degree of freedom is directly measured in various bases. The latter could be implemented, for example, with a Nitrogen Vacancy (NV) center-spin qubit in a nanodiamond crystal, where the spin state is rotated by a microwave pulse, which corresponds to basis change, followed by a fluorescence measurement by shining a laser resonant with an optical transition [64]. The implementation would require cryogenic temperature of the diamond [65,66]. So the spin coherence time is much greater than the experimental time scale [63]. As the spin measurement is very efficient, we only need to consider the resolutions δx, δt of the spatial qubit measurements so that the effective spatial Pauli X and Y operators are then projections onto a mixed state with phase angle ranging from $\theta - \frac{\delta\theta}{2}$ to $\theta + \frac{\delta\theta}{2}$ with $\delta\theta = \frac{md}{\hbar t_{\text{meas}}^{x,y}}\delta x - \frac{xmd}{\hbar(t_{\text{meas}}^{x,y})^2}\delta t$. For purposes of coherence, which continuously decreases with time, it is best to choose time of the order of the minimum allowed time for overlap of the wavepackets, i.e., choose $t_{\text{meas}}^{x,y} = d(2\sigma_d m)/\hbar$ so that $\delta\theta = \frac{\delta x}{2\sigma_d} - \frac{x\hbar}{4\sigma_d^2 md}\delta t$. The approximate Pauli matrices are then

$$\tilde{\sigma}_x = \frac{1}{\delta\theta}\begin{pmatrix} 0 & \int_{\theta-\frac{\delta\theta}{2}}^{\theta+\frac{\delta\theta}{2}} e^{-i\theta}d\theta|_{\theta=0} \\ \int_{\theta-\frac{\delta\theta}{2}}^{\theta+\frac{\delta\theta}{2}} e^{i\theta}d\theta|_{\theta=0} & 0 \end{pmatrix}$$

$$= \frac{1}{\delta\theta}\begin{pmatrix} 0 & -ie^{i\frac{\delta\theta}{2}} + ie^{-i\frac{\delta\theta}{2}} \\ -ie^{i\frac{\delta\theta}{2}} + ie^{-i\frac{\delta\theta}{2}} & 0 \end{pmatrix},$$

and similarly, $\tilde{\sigma}_y = \frac{1}{\delta\theta}\begin{pmatrix} 0 & -e^{i\frac{\delta\theta}{2}} + e^{-i\frac{\delta\theta}{2}} \\ e^{i\frac{\delta\theta}{2}} - e^{-i\frac{\delta\theta}{2}} & 0 \end{pmatrix}$. To verify the entanglement we have to show that the spin-motion entangled state violates the Bell-CHSH inequality $\mathcal{B} = |\langle AB\rangle + \langle AB'\rangle + \langle A'B\rangle - \langle A'B'\rangle| \leqslant 2$ with variables [67] $A = \tau_x + \tau_y$ and $A' = \tau_x - \tau_y$ operators of the spin (τ_x and τ_y are spin Pauli matrices) and $B = \tilde{\sigma}_x$ and $B' = \tilde{\sigma}_y$ operators of the spatial qubit. The expected correlation can be calculated (see Appendix) to give $\mathcal{B} = |2\sqrt{2}f(\delta\theta)| \leqslant 2\sqrt{2}$ where $f(\delta\theta) = \frac{2}{\delta\theta}\text{Re}[ie^{i\delta\theta/2}] = \frac{2}{\delta\theta}\cos(\frac{\pi+\delta\theta}{2})$. To obtain a violation of the CHSH inequality the upper bound of $\delta\theta$ can be calculated as $|f(\delta\theta)| = \frac{1}{\sqrt{2}}$, $\delta\theta \approx 2.783$. Due to high tolerance in spatial detection, one may pick $\delta\theta = \pi/2$ so that the four detectors consisting of Pauli X and Y measurements are placed adjacent to each other and cover the full range $\theta \in [-3/4\pi, 5/4\pi]$. The probability of detection is $\sim$17.7% for each repetition of the experiment.

For realization, consider a $m \sim 10^{-19}$ kg (10^8 amu) spin-bearing mass cooled to a ground state in $\omega \sim 1$ kHz trap [68,69] so that its ground-state spread is $= \sqrt{\frac{\hbar}{2m\omega}} \sim 1$ nm. The cooling to ground state essentially requires a measurement to the accuracy of the ground-state spread and sufficient isolation. Essentially, measuring the position of an object to the above precision (nm) requires 3×10^7 photons, which will hardly heat up the system in a diamagnetic trap. In fact, feedback cooling has been achieved for massive (10 kg) masses [70].

At time $t = 0$ the embedded spin is placed in a superposition $1/\sqrt{2}(|\uparrow\rangle + |\downarrow\rangle)$, and the mass is released from the trap. The wave packet then passes through an inhomogeneous magnetic field gradient $\sim 10^5$ Tm^{-1} [25]. Due to the Stern-Gerlach effect, the mass moves in opposite directions corresponding to

$|\uparrow\rangle$ and $|\downarrow\rangle$ spin states and, in a time-scale of $t_{\text{prep}} \sim 50$ μs, evolves to a $|\phi^+\rangle$ state with a separation of $d = 25$ nm between the $|0\rangle$ and $|1\rangle$ spatial qubit states [12,22,25–27] (all lower m and d are also possible as they demand lower t_{prep} and $\partial B/\partial x$). To keep the spin coherence for t_{prep}, dynamical decoupling may be needed [63]; it is possible to accommodate this within our protocols—one just needs to change the direction of the magnetic field as well in tandem with the dynamical decoupling pulses which flip the spin direction [71]. During the above t_{prep}, the spread of wavepackets is negligible so that σ_d remains $\sim$1 nm.

According to our results above, in order to obtain a CHSH inequality violation, one has to measure to within $\delta x \sim 2\sigma_d\delta\theta \sim 1$ nm resolution. To achieve this resolution, first we have to ensure that during the whole duration of our protocol, the acceleration noise has to be below a certain threshold so as to not cause random displacement greater than 1 nm. Given $t^{x,y} \sim 50$ ms is the longest duration step, the acceleration noise needs to be $\sim 10^{-6}$ ms^{-2}. Next comes the measurement step where light is scattered from the object, which also needs to measure to the required resolution. This is possible as there are feasible techniques that give resolutions of 0.1 pm/$\sqrt{\text{Hz}}$ [58,59] for position measurements by scattering light continuously from an object. Adopting the scheme in Ref. [59], the resolution can be achieved by scattering light continuously from the object for about 1 μs, which is 4 orders of magnitude smaller than the experimental time span. On the other hand if the timing accuracy δt of $t_{\text{meas}}^{x,y}$ is kept below $\sim$0.1 ms (also easy in terms of laser switching on/off times), there is a negligible inaccuracy in θ.

Note that as shown in the Appendix, dephasing between the spatial states $|0\rangle$ and $|1\rangle$ at a rate γ simply suppresses the CHSH violation by a factor $e^{-\gamma t}$, which could be a new way to investigate decoherence of the mass from various postulated models [16–21] and environment. As during the preparation of the superposition, spatial states are in one-to-one correspondence with spin states ($|0\uparrow\rangle$, $|1\downarrow\rangle$), the spin decoherence affects the superposition in the same way, and their effect is mathematically captured by the same γ.

The decoherence of the spatial degree of freedom results from background gas collision and black-body radiation. Adopting the formulas from Ref. [10], for our realization, the contribution to γ from background gas reaches $\sim$167.2 s^{-1} at pressure $\sim 10^{-10}$ Torr. Black-body radiation induces decoherence at a rate of $\sim$274.9 s^{-1} at internal temperature 50 K. On the other hand, the spin degree of freedom, which may be encoded in NV centers of nanodiamond crystal, reaches a coherence time of $\sim$0.6 s at liquid nitrogen temperature 77 K [63]. As it stands, the coherence of electron spins in nanodiamonds is lower than what we require for 10^{-19} kg mass [72–74]. However, recently, much larger times of 0.4 ms has been achieved via dynamical decoupling [75]. This is already much larger than the superposition state preparation time ($\sim$50 μs). There are ideas to incorporate dynamical decoupling in the preparation of the initial superposition in our experiment [71]. There are also ideas of using bath dynamical decoupling which should not affect the spatial superposition generation [76]. Note that, strictly speaking, the electronic spin is only required during the Stern-Gerlach generation of superposition after which it can be mapped onto nuclear
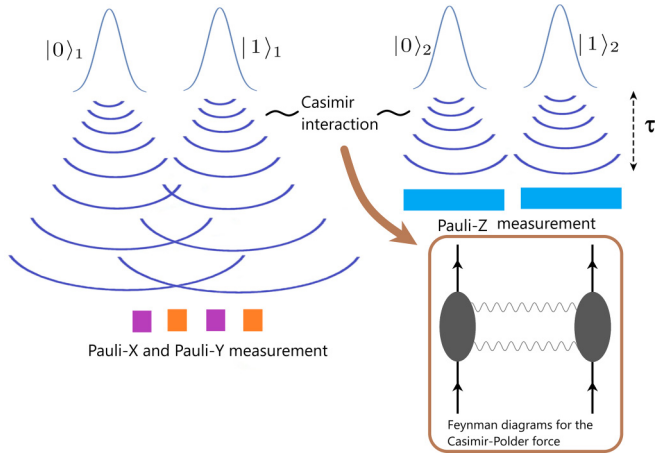
FIG. 3. Application in witnessing Casimir-induced entanglement: Two masses, each prepared in a superposition of two states, act as two qubits $\frac{1}{\sqrt{2}}(|0\rangle_1 + |1\rangle_1) \otimes \frac{1}{\sqrt{2}}(|0\rangle_2 + |1\rangle_2)$. The system freely propagates and undergoes mutual interactions for a time τ. This interaction induces entanglement which can be witnessed from correlations of spatial qubit Pauli measurements. For example, in the figure, σ_x, σ_y measurements on test mass 1 and σ_z measurements on test mass 2 are depicted. Casimir interaction induced by virtual photons as quantum mediators is shown [79].

spins. Before the free packet expansion (interferometry), the electronic spin can be mapped onto nuclear spin which has much longer coherence times. At the end of the protocol, we will need to measure the nuclear spin, for which we may need to map back to electronic state. Such mapping can happen in microseconds given the hyperfine couplings [77]. Therefore, achievable pressure and temperature make the coherence time sufficient for the realization of our protocol (same estimates hold for the protocol of the next section).

As *both* the spin and the mass are measured, it characterizes the entanglement of the given state *irrespective* of the dynamics from which the state was generated, as opposed to previous protocols which rely on a reversible nature of the quantum dynamics [3–6]. As opposed to single object interferometry [10,55,56], here the CHSH violation explores decoherence of the mass in multiple bases—not only how the $|0\rangle\langle1|$ term of the spatial qubit decays (position basis), but also whether, and if so how, $|+\rangle\langle-|$ decays (where $|-\rangle = |0\rangle - |1\rangle$)—a novel type of decoherence of even/odd parity basis. Moreover, as the total spin-motional system is quantum 4 state system, the CHSH violation can also be regarded as a violation of the classical notion of noncontextuality [34,35,78].

IV. CASIMIR-INDUCED ENTANGLEMENT

Neutral unmagnetized untrapped masses, ideal for the preservation of spatial coherence, can interact with each other via the Casimir interaction [26] (gravity can cause observable effects in reasonable times only for masses $>10^{-15} - 10^{-14}$ kg [22,26]). Two such masses (mass m, radius R) indexed 1 and 2 are each prepared in the spatial qubit state $|+\rangle$ (the superposition size, separation between states $|0\rangle$ and $|1\rangle$, being d) while the distance between the centers of the superpositions is D (Fig. 3). In a time τ, the Casimir

interaction evolves the system to

$$\frac{e^{i\phi}}{\sqrt{2}}\left[|0\rangle_1 \frac{1}{\sqrt{2}}(|0\rangle_2 + e^{i\Delta\phi_{01}}|1\rangle_2) + |1\rangle_1 \frac{1}{\sqrt{2}}(e^{i\Delta\phi_{10}}|0\rangle_2 + |1\rangle_2)\right],$$

(4)

where $\phi = k\frac{R^6}{D^7}\tau$, $\Delta\phi_{01} = k\frac{R^6}{(D+d)^7}\tau - \phi$, $\Delta\phi_{10} = k\frac{R^6}{(D-d)^7}\tau - \phi$, in which $k = \frac{23c}{4\pi}(\epsilon - 1)^2/(\epsilon + 2)^2$ [80] (See also Refs. [81,82]), where ϵ is the dielectric constant of the material of the masses. This formula is valid when the separation is much larger than the radius of the sphere, which is the regime of our subsequent calculations. On top of the above evolution, we assume a local dephasing $|0\rangle\langle1|_i \rightarrow e^{-\gamma\tau}|0\rangle\langle1|_i$ for both particles $i = 1, 2$ (this can generically model all dephasing [26,83]). To verify the induced entanglement, one can make spatial qubit measurements up to uncertainties parametrized by $\delta\theta$ as outlined previously and then estimate the entanglement witness [84] $W = I \otimes I - \tilde\sigma_x \otimes \tilde\sigma_x - \tilde\sigma_z \otimes \tilde\sigma_y - \tilde\sigma_y \otimes \tilde\sigma_z$ where $\tilde\sigma_x$ and $\tilde\sigma_y$ are as discussed before, and we take $\tilde\sigma_z = \int_{-\infty}^0 |x\rangle\langle x|dx - \int_0^\infty |x\rangle\langle x|dx$. If $\langle W\rangle = \text{Tr}(W\rho)$ is negative, the masses are entangled. We find

$$\langle\tilde{W}\rangle = 1 - \frac{1}{2}e^{-2\gamma t}g^2(\delta\theta)(1 + \cos(\Delta\phi_{10} - \Delta\phi_{01}))$$
$$- e^{-\gamma t}g(\delta\theta)(\sin(\Delta\phi_{10}) + \sin(\Delta\phi_{01})), \quad (5)$$

where $g(\delta\theta) = \frac{2}{\delta\theta}\cos(\frac{\pi - \delta\theta}{2})$.

We are going to consider the Stern-Gerlach mechanism to first prepare the state $|\phi^+\rangle$, and use that to prepare $|+\rangle$. We consider a $R \sim 20$ nm, $m \sim 1.17 \times 10^{-19}$ kg mass, and consider it to have been trapped and cooled it to its ground state $\sigma_d \sim 1$ nm in a 1 kHz trap [56]. We then release it, and subject it to a magnetic field gradient of 5×10^4 Tm^{-1} [25] for $t \sim 100$ μs so that a Stern-Gerlach splitting of $d \approx 50$ nm develops while there is insignificant wavepacket spreading (σ_d remains $\sim$1 nm). At this stage, a microwave pulse may be given to rotate the spin state so that the $|\phi^+\rangle$ state evolves to $|0\rangle(|\uparrow\rangle + |\downarrow\rangle) + |1\rangle(|\uparrow\rangle - |\downarrow\rangle)$. A subselection of the $|\uparrow\rangle$ spin state via deflection through another Stern-Gerlach then yields the state $|+\rangle$ [31,33]. Alternatively, by performing a controlled-NOT gate with the spatial qubit as the control and the spin as the target (again, performed quite accurately by a microwave pulse [56]), $|\phi^+\rangle$ gets converted to $|+\rangle|\downarrow\rangle$ so that the spatial part is our required state. For $D \approx 2.1$ μm, then $\Delta\phi_{10} = \phi_{10} - \phi \approx 0.17$, $\Delta\phi_{01} = \phi_{01} - \phi \approx -0.14$ after $\tau \sim 0.012$ s of entangling time, which gives a negative witness $\langle W\rangle \sim -0.0064$. A value of $\delta\theta \sim \pi/6$ is the highest tolerance of error in spatial detection to keep the entanglement witness negative. The position detectors that consist of Pauli X and Y measurements with width $\delta\theta \sim \pi/6$ has $\sim$5.9% chance of detection for each repetition of the experiment.

Note here that the form of witness operator compels one to measure both the $\tilde\sigma_x \otimes \tilde\sigma_x$ operator and the other two operators on the *same entangled state*. $\tilde\sigma_z$ measurement is also done at $t_{\text{meas}}^z = \tau$. This is about 0.1 of the overlapping time $\sim\frac{d(2\sigma_d m)}{\hbar}$ so that the fidelity of the σ_z measurement is very high (see Appendix). We then require $t_{\text{meas}}^{x,y} - t_{\text{meas}}^z \ll \tau$ so that the extra entanglement generated due to interactions after the $\tilde\sigma_z$ measurement and before the $\tilde\sigma_x/\tilde\sigma_y$ measurements is negligible. This in turn requires us to *speed up* the development of spatial overlap between the qubit states due to wavepacket spreading

after the $\tilde{\sigma}_z$ measurement, which can be accomplished by squeezing both of the wavepackets in position after the time t_{meas}^z. After 0.01 s of flight, the wavepacket width $\sigma_d \sim 1$ nm expands to ~ 10 nm. Thus we have to squeeze the state by 2 orders of magnitude to $\sim 1 \times 10^{-10}$ m, so that it expands to ~ 100 nm, where overlapping occurs, in the next 0.001 s. The fidelity of XY measurement here is very high (see Appendix). The slight delay in $\sigma_{x/y}$ measurement (0.001 s later than the σ_z measurement) would cause only a $\sim 5\%$ error in the witness magnitude. Note that in order to achieve the required squeezing, two appropriate periods of unitary evolution in harmonic potentials of $\omega_1 \sim 1$ MHz and $\omega_2 \sim 0.1$ MHz would suffice (n repeated changes between ω_1 and ω_2 separated by appropriate periods of harmonic evolution will squeeze by the factor $(\omega_1/\omega_2)^n$ [85]); if this potential was applied as an optical tweezer then it will hardly cause any decoherence $\gamma_{\text{squeeze},j} \sim \omega_j 10^{-5}$ [7]. We additionally need to ensure, for reasons described earlier, that the acceleration noise is below 10^{-6} ms^{-2}. The whole procedure described above could be one of the earliest demonstrations of non-Gaussian entanglement between neutral masses. It would also demonstrate the nonclassical nature of the Casimir interaction, namely that it is mediated by quantum agents (virtual photons) as in the inset of Fig. 3.

Compared with other types of interactions, gravitational interaction at this scale is negligible compared with Casimir interaction as long as the separation between the two masses are less than 200 μm for materials with density of diamonds [22]. The phase induced by electrostatic interaction can be estimated by $\frac{\vec{p}^2 t}{4\pi\epsilon_0 R^3 \hbar}$, where $\vec{p}$ is electric dipole moment. For $R \sim 20$ nm, $t \sim 10$ ms, $\vec{p}$ needs to be much smaller than 10^{-30} C.m to be considered negligible compared with Casimir interaction. In current experiments, $\vec{p}$ can be as small as $\sim 10^{-23}$ C.m for 10 μm radius particles, scaling with the volume of the particle [86,87]. From the scaling, we can expect electric dipole $\sim 10^{-29}$ C.m for 10 nm radius particles. An improvement of the electric dipole by a couple of orders of magnitude is required to make electrostatic interaction negligible in comparison with Casimir interaction. These electric dipoles typically appear due to defects in crystals such as dislocations. It is possible that given the 10 nm size, one can form a single crystal [88] so that the intrinsic dipole background can be reduced.

V. CONCLUSIONS

We have shown how to measure a qubit encoded in a massive object by position detection. We have shown how this can be applied to (a) stretch the validity of quantum physics to the center of mass of nano-objects, demonstrating quantum contextuality, never before tested for macroscopic objects, (b) entangle spatial qubits encoded in two such objects, extending non-Gaussian quantum technology, (c) prove empirically the quantum coherent nature of the Casimir force. Indeed, in the *same* open-minded way that one asks whether quantum mechanics continues to hold for macroscopic masses [1,2], one can question whether those interactions between such masses which are extensive in nature (grow as volume/area/mass) *continue* to be mediated by a quantum natured field so as to

be able to entangle the masses. In comparison with standard approaches for probing the nonclassicality for smaller masses, we avoid a Mach-Zehnder interferometer—only requiring the preparation of an original spatial superposition. This is advantageous because of the difficulty of realizing beam splitters for nano-objects (tunneling probability $\propto e^{-\frac{\sqrt{2mV}}{\hbar}\Delta x}$ getting extremely small), and also for avoiding interactions with mirrors and beam splitters which can cause decoherence (we exploit a two-slit experiment as a beam-splitter [89], see Appendix E). Our methodology can be quantum mechanically simulated with cold atoms, where other methods to encode qubits in motional states have been demonstrated [90], before they are actually applied to nano-objects.

APPENDIX A: EFFICACY OF THE PAULI-Z MEASUREMENT AS A FUNCTION OF MEASUREMENT TIME

The system freely propagates for a time t, the final state may be written for an initial state $|+\rangle$ as

$$\langle x|\Psi(t)\rangle = \frac{1}{[2\pi\sigma^2]^{1/4}}\sqrt{\frac{1}{\frac{1}{s} - i\frac{\hbar t}{2m}}} \left\{ \exp\left[-\frac{\left(x - \frac{d}{2\sigma_d^2 s}\right)^2}{4\left(\frac{1}{s} - i\frac{\hbar t}{2m}\right)} \right] + \exp\left[-\frac{\left(x + \frac{d}{2\sigma_d^2 s}\right)^2}{4\left(\frac{1}{s} - i\frac{\hbar t}{2m}\right)} \right] \right\}, \tag{A1}$$

where $s \equiv \frac{i4\phi}{\sigma^2} + \frac{1}{\sigma^2} + \frac{1}{\sigma_d^2}$, ϕ is global phase added during the propagation.

Note that Eq. (A1) consists of two terms tracing which path the object passes through, effectively the predefined Young qubit. σ_z measurement requires that the wavepackets are well separated upon measurement. The condition maybe formulated by demanding the probability distribution P_0 (P_1) of $|0\rangle$ ($|1\rangle$) state alone confined in the $x < 0$($x > 0$) regime

$$\epsilon = 1 - \frac{\int_{-\infty}^0 P_0 dx}{\int_{-\infty}^\infty P_0 dx} \ll 1. \tag{A2}$$

Substituting Eq. (A1), the fraction term can be evaluated at the σ_z measurement time $t = t_{\text{meas}}^z$:

$$\frac{\int_{-\infty}^0 P_0 dx}{\int_{-\infty}^\infty P_0 dx} = \frac{\int_{-\infty}^0 \exp\left[-\frac{(x + \frac{d}{2\sigma_d^2 s})^2 \frac{1}{s}}{\frac{2}{s^2} + \frac{\hbar^2 t^2}{8m^2}} \right] dx}{\int_{-\infty}^\infty \exp\left[-\frac{(x + \frac{d}{2\sigma_d^2 s})^2 \frac{1}{s}}{\frac{2}{s^2} + \frac{\hbar^2 t^2}{8m^2}} \right] dx}, \tag{A3}$$

where the normalization factor in the probability distribution, independent of x, cancels out in the calculation.

Let us take $\sigma_d : d = 1 : 50$ and $t^z_{\text{meas}} \approx$ one-tenth of the overlapping time $\frac{d(2\sigma_d m)}{\hbar}$. We then get $\epsilon \sim (1 - 4.7 \times 10^{-7})$. We may thus claim that for the above choice of parameters the left and right Gaussian wavepackets are well separated, and Pauli-Z measurement has a good fidelity.

APPENDIX B: EFFICACY OF THE PAULI-*X* AND PAULI-*Z* MEASUREMENT FOR VARIOUS PARAMETERS

We take $t = t^{x,y}_{\text{meas}} \sim \frac{2\sigma_d m d}{\hbar}$ as the time of σ_x, σ_y measurement, and evaluate how accurate this measurement is for various ratios $\sigma_d : d$ using the full-time evolution as in Eq. (A1). Our target is to check how accurately the interference pattern is reproduced at correct positions as given by $x = \frac{\hbar k_x t^{x,y}_{\text{meas}}}{m}$. For an initial state $|0\rangle + |1\rangle$, if $\sigma_d : d = 1 : 10$ the first peak of the interference pattern adjacent to the central peak (corresponding to $\theta = 2\pi$) locates at $x \sim 11.797\sigma_d$. If $\sigma_d : d = 1 : 100$, $x \sim 12.559\sigma_d$. If $\sigma_d : d = 1 : 50$, $x \sim 12.536\sigma_d$. While assumption $x = \frac{\hbar k_x t^{x,y}_{\text{meas}}}{m}$ gives a value of $x = 4\pi\sigma_d \sim 12.566\sigma_d$, which is $> \sim 99.94\%$ accurate for $\frac{\sigma_d}{d} \leqslant \frac{1}{100}$, $> \sim 99.76\%$ accurate for $\frac{\sigma_d}{d} \leqslant \frac{1}{50}$. Therefore, the σ_x, σ_y measurements have a good fidelity in the $\frac{\sigma_d}{d} \leqslant \frac{1}{50}$ setting, which we shall use.

APPENDIX C: METHODS OF COMPUTATION WITH EFFECTIVE PAULI OPERATORS INCLUDING UNCERTAINTIES, AND THE INCORPORATION OF DECOHERENCE

Let $\tilde{\sigma}$ denote the measured Pauli operator, parametrized by uncertainty in phase angle $\delta\theta$. Then,

$$\tilde{\sigma}_x = \frac{1}{\delta\theta} \begin{pmatrix} 0 & -ie^{i\frac{\delta\theta}{2}} + ie^{-i\frac{\delta\theta}{2}} \\ -ie^{i\frac{\delta\theta}{2}} + ie^{-i\frac{\delta\theta}{2}} & 0 \end{pmatrix}$$
$$= g(\delta\theta)\sigma_x, \qquad (C1)$$

where $g(\delta\theta) = -ie^{i\frac{\delta\theta}{2}} + ie^{-i\frac{\delta\theta}{2}} = \frac{2}{\delta\theta}\cos(\frac{\pi - \delta\theta}{2})$. $g(\delta\theta)$ goes to 1 as $\delta\theta \to 0$. Similarly,

$$\tilde{\sigma}_y = g(\delta\theta)\sigma_y. \qquad (C2)$$

Therefore, for arbitrary density state ρ

$$Tr(\tilde{\sigma}_x\rho) = g(\delta\theta)Tr(\sigma_x\rho),$$
$$Tr(\tilde{\sigma}_y\rho) = g(\delta\theta)Tr(\sigma_y\rho). \qquad (C3)$$

In particular, let $\rho_{x+}(\rho_{y+})$ denote the positive eigenstate of $\sigma_x(\sigma_y)$, and $\rho_{x+} = \frac{1}{2}\begin{pmatrix} 1 & 1 \\ 1 & 1 \end{pmatrix}$, $\rho_{y+} = \frac{1}{2}\begin{pmatrix} 1 & -i \\ i & 1 \end{pmatrix}$. Then,

$$Tr(\tilde{\sigma}_x\rho_{x+}) = Tr(\tilde{\sigma}_y\rho_{y+}) = g(\delta\theta). \qquad (C4)$$

Furthermore, if decoherence is considered, let $\tilde{\rho} = \begin{pmatrix} \rho_{00} & \rho_{01}e^{-\gamma t} \\ \rho_{10}e^{-\gamma t} & \rho_{11} \end{pmatrix}$, where γ denotes dephasing rate, then we have

$$\text{Tr}(\tilde{\sigma}_x\tilde{\rho}) = g(\delta\theta)Tr(\sigma_x\rho)e^{-\gamma t},$$
$$\text{Tr}(\tilde{\sigma}_y\tilde{\rho}) = g(\delta\theta)Tr(\sigma_y\rho)e^{-\gamma t}. \qquad (C5)$$

APPENDIX D: DECOHERENCE IN PROBING THE ENTANGLEMENT OF THE STERN-GERLACH STATE

Consider the initial state $|\phi^+\rangle = \frac{1}{\sqrt{2}}(|\uparrow, R\rangle + |\downarrow, L\rangle)$, where the spatial qubit undergoes decoherence. The density operator after decoherence can be written as

$$\tilde{\rho}(\phi^+) = \frac{1}{2} \begin{pmatrix} 0 & 0 & 0 & 0 \\ 0 & 1 & e^{-\gamma t} & 0 \\ 0 & e^{-\gamma t} & 1 & 0 \\ 0 & 0 & 0 & 0 \end{pmatrix}, \qquad (D1)$$

$$\text{Tr}(\sigma_x \otimes \sigma_x\tilde{\rho}(\phi^+)) = \text{Tr}(\sigma_y \otimes \sigma_y\tilde{\rho}(\phi^+)) = e^{-\gamma t},$$
$$\text{Tr}(\sigma_x \otimes \sigma_y\tilde{\rho}(\phi^+)) = \text{Tr}(\sigma_y \otimes \sigma_x\tilde{\rho}(\phi^+)) = 0. \qquad (D2)$$

Therefore,

$$|\langle ab\rangle + \langle ab'\rangle + \langle a'b\rangle - \langle a'b'\rangle| = |2\sqrt{2}g(\delta\theta)e^{-\gamma t}| \leqslant 2\sqrt{2}. \qquad (D3)$$

APPENDIX E: YOUNG-TYPE QUBIT AS BEAM SPLITTER

Our experimental setup serves the same purpose as a Mach-Zehnder interferometer in probing contextuality [34], in which a particle passes through beam splitters and which path information defines a spatial qubit. In our approach, a Young-type double slit acts effectively as a lossy beam splitter [89]. A cubic beam splitter has two input and two output. The transformation matrix from the former to the latter ports is described by a two-by-two unitary matrix. The initial states $|0\rangle$ and $|1\rangle$ act as the two input. By placing a pair of detectors in the interference plane, we project the input states onto a different basis, parametrized by phase angle θ. For instance, conducting Pauli-*Y* operation requires placing two detectors at phase angle $-\pi/2$ and $\pi/2$ respectively. The effective beam splitter therefore transforms the system from a superposition of $|0\rangle$ and $|1\rangle$ to the basis spanned by $|0\rangle - i|1\rangle$ and $|0\rangle + i|1\rangle$. The transformation matrix is therefore $\frac{1}{\sqrt{2}}\begin{pmatrix} 1 & i \\ 1 & -i \end{pmatrix} = \frac{1}{\sqrt{2}}\begin{pmatrix} 1 & i \times e^{-i\pi/2} \\ 1 \times e^{-i\pi/2} \end{pmatrix}$, equivalently, a 50:50 beam splitter followed by a phase shifter with angle $-\pi/2$.

[1] A. J. Leggett, Testing the limits of quantum mechanics: motivation, state of play, prospects, J. Phys.: Condens. Matter **14**, R415 (2002).

[2] M. Arndt, K. Hornberger, and A. Zeilinger, Probing the limits of the quantum world, Phys. World **18**, 35 (2005).

[3] S. Bose, K. Jacobs, and P. L. Knight, Scheme to probe the decoherence of a macroscopic object, Phys. Rev. A **59**, 3204 (1999).

[4] A. Armour, M. P. Blencowe, and K. C. Schwab, Entanglement and Decoherence of a Micromechanical Resonator via Coupling to a Cooper-Pair Box, Phys. Rev. Lett. **88**, 148301 (2002).

[5] W. Marshall, C. Simon, R. Penrose, and D. Bouwmeester, Towards Quantum Superpositions of a Mirror, Phys. Rev. Lett. **91**, 130401 (2003).

[6] S. Bose, Qubit Assisted Probing of Coherence between Mesoscopic States of an Apparatus, Phys. Rev. Lett. **96**, 060402 (2006).

[7] D. E. Chang, C. Regal, S. Papp, D. Wilson, J. Ye, O. Painter, H. J. Kimble, and P. Zoller, Cavity opto-mechanics using an optically levitated nanosphere, Proc. Natl. Acad. Sci. USA **107**, 1005 (2010).

[8] O. Romero-Isart, M. L. Juan, R. Quidant, and J. I. Cirac, Toward quantum superposition of living organisms, New J. Phys. **12**, 033015 (2010).

[9] O. Romero-Isart, A. C. Pflanzer, F. Blaser, R. Kaltenbaek, N. Kiesel, M. Aspelmeyer, and J. I. Cirac, Large Quantum Superpositions and Interference of Massive Nanometer-Sized Objects, Phys. Rev. Lett. **107**, 020405 (2011).

[10] O. Romero-Isart, Quantum superposition of massive objects and collapse models, Phys. Rev. A **84**, 052121 (2011).

[11] M. Scala, M. S. Kim, G. W. Morley, P. F. Barker, and S. Bose, Matter-Wave Interferometry of a Levitated Thermal Nano-Oscillator Induced and Probed by a Spin, Phys. Rev. Lett. **111**, 180403 (2013).

[12] C. Wan, M. Scala, G. W. Morley, ATM. A. Rahman, H. Ulbricht, J. Bateman, P. F. Barker, S. Bose, and M. S Kim, Free Nano-Object Ramsey Interferometry for Large Quantum Superpositions, Phys. Rev. Lett. **117**, 143003 (2016).

[13] S. Bose, D. Home, and S. Mal, Nonclassicality of the Harmonic-Oscillator Coherent State Persisting up to the Macroscopic Domain, Phys. Rev. Lett. **120**, 210402 (2018).

[14] S. Gerlich, S. Eibenberger, M. Tomandl, S. Nimmrichter, K. Hornberger, P. J. Fagan, J. Tüxen, M. Mayor, and M. Arndt, Quantum interference of large organic molecules, Nat. Commun. **2**, 263 (2011).

[15] Y. Y. Fein, P. Geyer, P. Zwick, F. Kiałka, S. Pedalino, M. Mayor, S. Gerlich, and M. Arndt, Quantum superposition of molecules beyond 25 kda, Nat. Phys. **15**, 1242 (2019).

[16] L. Diósi, Models for universal reduction of macroscopic quantum fluctuations, Phys. Rev. A **40**, 1165 (1989).

[17] R. Penrose, On gravity's role in quantum state reduction, Gen. Relativ. Gravit. **28**, 581 (1996).

[18] A. Bassi, K. Lochan, S. Satin, T. P. Singh, and H. Ulbricht, Models of wave-function collapse, underlying theories, and experimental tests, Rev. Mod. Phys. **85**, 471 (2013).

[19] G. J. Milburn, Intrinsic decoherence in quantum mechanics, Phys. Rev. A **44**, 5401 (1991).

[20] J. Oppenheim, A post-quantum theory of classical gravity? arXiv:1811.03116.

[21] S. Weinberg, Collapse of the state vector Phys. Rev. A **85**, 062116 (2012).

[22] S. Bose, A. Mazumdar, G. W. Morley, H. Ulbricht, M. Toroš, M. Paternostro, A. A. Geraci, P. F. Barker, M. Kim, and G. Milburn, Spin Entanglement Witness for Quantum Gravity, Phys. Rev. Lett. **119**, 240401 (2017).

[23] R. J. Marshman, A. Mazumdar, and S. Bose, Locality and entanglement in table-top testing of the quantum nature of linearized gravity, Phys. Rev. A **101**, 052110 (2020).

[24] C. Marletto and V. Vedral, Gravitationally Induced Entanglement between Two Massive Particles is Sufficient Evidence of Quantum Effects in Gravity, Phys. Rev. Lett. **119**, 240402 (2017).

[25] Y. Margalit, O. Dobkowski, Z. Zhou, O. Amit, Y. Japha, S. Moukouri, D. Rohrlich, A. Mazumdar, S. Bose, C. Henkel *et al.*, Realization of a complete Stern-Gerlach interferometer: Towards a test of quantum gravity, Sci. Adv. **7**, eabg2879 (2021).

[26] T. W. van de Kamp, R. J. Marshman, S. Bose, and A. Mazumdar, Quantum gravity witness via entanglement of masses: Casimir screening, Phys. Rev. A **102**, 062807 (2020).

[27] R. J. Marshman, A. Mazumdar, G. W. Morley, P. F. Barker, S. Hoekstra, and S. Bose, Mesoscopic interference for metric and curvature & gravitational wave detection, New J. Phys. **22**, 083012 (2020).

[28] B. Englert, J. Schwinger, and M. Scully, Is spin coherence like humpty-dumpty? I. simplified treatment, Found Phys. **18**, 1045 (1988).

[29] D. Home, A. K. Pan, M. M. Ali, and A. Majumdar, Aspects of nonideal stern–gerlach experiment and testable ramifications, J. Phys. A: Math. Theor. **40**, 13975 (2007).

[30] M. Keil, S. Machluf, Y. Margalit, Z. Zhou, O. Amit, O. Dobkowski, Y. Japha, S. Moukouri, D. Rohrlich, Z. Binstock *et al.*, Stern-gerlach interferometry with the atom chip, arXiv:2009.08112.

[31] Y. Margalit, Z. Zhou, S. Machluf, Y. Japha, S. Moukouri, and R. Folman, Analysis of a high-stability stern–gerlach spatial fringe interferometer, New J. Phys. **21**, 073040 (2019).

[32] E. Rosenfeld, R. Riedinger, J. Gieseler, M. Schuetz, and M. D. Lukin, Efficient Entanglement of Spin Qubits Mediated by a Hot Mechanical Oscillator, Phys. Rev. Lett. **126**, 250505 (2021).

[33] S. Machluf, Y. Japha, and R. Folman, Coherent stern–gerlach momentum splitting on an atom chip, Nat. Commun. **4**, 2424 (2013).

[34] S. Basu, S. Bandyopadhyay, G. Kar, and D. Home, Bell's inequality for a single spin-1/2 particle and quantum contextuality, Phys. Lett. A **279**, 281 (2001).

[35] D. Home and S. Sengupta, Bell's inequality and non-contextual dispersion-free states, Phys. Lett. A **102**, 159 (1984).

[36] S. K. Lamoreaux, The casimir force and related effects: The status of the finite temperature correction and limits on new long-range forces, Annu. Rev. Nucl. Part. Sci. **62**, 37 (2012).

[37] Z. Xu and T. Li, Detecting casimir torque with an optically levitated nanorod, Phys. Rev. A **96**, 033843 (2017).

[38] Z. Xu, X. Gao, J. Bang, Z. Jacob, and T. Li, Non-reciprocal energy transfer through the Casimir effect, Nat. Nanotech. **17**, 148 (2022).

[39] S. Osnaghi, P. Bertet, A. Auffeves, P. Maioli, M. Brune, J.-M. Raimond, and S. Haroche, Coherent Control of an Atomic Collision in a Cavity, Phys. Rev. Lett. **87**, 037902 (2001).

[40] A. J. Landig, J. V. Koski, P. Scarlino, C. Müller, J. C. Abadillo-Uriel, B. Kratochwil, C. Reichl, W. Wegscheider, S. N. Coppersmith, M. Friesen *et al.*, Virtual-photon-mediated

spin-qubit–transmon coupling, Nat. Commun. **10**, 5037 (2019).

[41] D. Kafri and J. Taylor, A noise inequality for classical forces, arXiv:1311.4558.

[42] T. Krisnanda, M. Zuppardo, M. Paternostro, and T. Paterek, Revealing Nonclassicality of Inaccessible Objects, Phys. Rev. Lett. **119**, 120402 (2017).

[43] S. Qvarfort, S. Bose, and A. Serafini, Mesoscopic entanglement through central–potential interactions, J. Phys. B: At., Mol. Opt. Phys. **53**, 235501 (2020).

[44] T. Krisnanda, G. Y. Tham, M. Paternostro, and T. Paterek, Observable quantum entanglement due to gravity, npj Quantum Inf. **6**, 12 (2020).

[45] T. Weiss, M. Roda-Llordes, E. Torrontegui, M. Aspelmeyer, and O. Romero-Isart, Large Quantum Delocalization of a Levitated Nanoparticle Using Optimal Control: Applications for Force Sensing and Entangling Via Weak Forces, Phys. Rev. Lett. **127**, 023601 (2021).

[46] R. Simon, Peres-Horodecki Separability Criterion for Continuous Variable Systems, Phys. Rev. Lett. **84**, 2726 (2000).

[47] G. Taguchi, T. Dougakiuchi, N. Yoshimoto, K. Kasai, M. Iinuma, H. F. Hofmann, and Y. Kadoya, Measurement and control of spatial qubits generated by passing photons through double slits, Phys. Rev. A **78**, 012307 (2008).

[48] D. Ghosh, T. Jennewein, P. Kolenderski, and U. Sinha, Spatially correlated photonic qutrit pairs using pump beam modulation technique, OSA Continuum **1**, 996 (2018).

[49] R. Sawant, J. Samuel, A. Sinha, S. Sinha, and U. Sinha, Nonclassical Paths in Quantum Interference Experiments, Phys. Rev. Lett. **113**, 120406 (2014).

[50] P. Kolenderski, U. Sinha, L. Youning, T. Zhao, M. Volpini, A. Cabello, R. Laflamme, and T. Jennewein, Aharon-vaidman quantum game with a young-type photonic qutrit, Phys. Rev. A **86**, 012321 (2012).

[51] G. Rengaraj, U. Prathwiraj, S. N. Sahoo, R. Somashekhar, and U. Sinha, Measuring the deviation from the superposition principle in interference experiments, New J. Phys. **20**, 063049 (2018).

[52] P. F. Barker and M. Shneider, Cavity cooling of an optically trapped nanoparticle, Phys. Rev. A **81**, 023826 (2010).

[53] U. Delić, M. Reisenbauer, K. Dare, D. Grass, V. Vuletić, N. Kiesel, and M. Aspelmeyer, Cooling of a levitated nanoparticle to the motional quantum ground state, Science **367**, 892 (2020).

[54] F. Tebbenjohanns, M. Frimmer, A. Militaru, V. Jain, and L. Novotny, Cold Damping of an Optically Levitated Nanoparticle to Microkelvin Temperatures, Phys. Rev. Lett. **122**, 223601 (2019).

[55] J. Bateman, S. Nimmrichter, K. Hornberger, and H. Ulbricht, Near-field interferometry of a free-falling nanoparticle from a point-like source, Nat. Commun. **5**, 4788 (2014).

[56] Z.-Q. Yin, T. Li, X. Zhang, and L. M. Duan, Large quantum superpositions of a levitated nanodiamond through spin-optomechanical coupling, Phys. Rev. A **88**, 033614 (2013).

[57] D. Gottesman, A. Kitaev, and J. Preskill, Encoding a qubit in an oscillator, Phys. Rev. A **64**, 012310 (2001).

[58] J. Gieseler, B. Deutsch, R. Quidant, and L. Novotny, Subkelvin Parametric Feedback Cooling of a Laser-Trapped Nanoparticle, Phys. Rev. Lett. **109**, 103603 (2012).

[59] J. Vovrosh, M. Rashid, D. Hempston, J. Bateman, M. Paternostro, and H. Ulbricht, Parametric feedback cooling of levitated optomechanics in a parabolic mirror trap, J. Opt. Soc. Am. B **34**, 1421 (2017).

[60] C. Caves, Defense of the Standard Quantum Limit for Free-Mass Position, Phys. Rev. Lett. **54**, 2465 (1985).

[61] Y. Hasegawa, R. Loidl, G. Badurek, M. Baron, and H. Rauch, Quantum Contextuality in a Single-Neutron Optical Experiment, Phys. Rev. Lett. **97**, 230401 (2006).

[62] S. Azzini, S. Mazzucchi, V. Moretti, D. Pastorello, and L. Pavesi, Single-particle entanglement, Adv. Quantum Technol. **3**, 2000014 (2020).

[63] N. Bar-Gill, L. M. Pham, A. Jarmola, D. Budker, and R. L. Walsworth, Solid-state electronic spin coherence time approaching one second, Nat. Commun. **4**, 1743 (2013).

[64] B. Hensen, H. Bernien, A. E. Dréau, A. Reiserer, N. Kalb, M. S. Blok, J. Ruitenberg, R. F. Vermeulen, R. N. Schouten, C. Abellán *et al.*, Loophole-free bell inequality violation using electron spins separated by 1.3 kilometres, Nature (London) **526**, 682 (2015).

[65] J.-W. Zhou, P.-F. Wang, F.-Z. Shi, P. Huang, X. Kong, X.-K. Xu, Q. Zhang, Z.-X. Wang, X. Rong, and J.-F. Du, Quantum information processing and metrology with color centers in diamonds, Front. Phys. **9**, 587 (2014).

[66] J.-F. Wang, F.-F. Yan, Q. Li, Z.-H. Liu, H. Liu, G.-P. Guo, L.-P. Guo, X. Zhou, J.-M. Cui, J. Wang *et al.*, Coherent Control of Nitrogen-Vacancy Center Spins in Silicon Carbide at Room Temperature, Phys. Rev. Lett. **124**, 223601 (2020).

[67] J. F. Clauser, M. A. Horne, A. Shimony, and R. A. Holt, Proposed Experiment to Test Local Hidden Variable Theories., Phys. Rev. Lett. **24**, 549 (1970).

[68] D. Zheng, Y. Leng, X. Kong, R. Li, Z. Wang, X. Luo, J. Zhao, C.-K. Duan, P. Huang, J. Du *et al.*, Room temperature test of the continuous spontaneous localization model using a levitated micro-oscillator, Phys. Rev. Res. **2**, 013057 (2020).

[69] Y. Leng, R. Li, X. Kong, H. Xie, D. Zheng, P. Yin, F. Xiong, T. Wu, C.-K. Duan, Y. Du *et al.*, Mechanical Dissipation Below 1 μ Hz with a Cryogenic Diamagnetic Levitated Micro-Oscillator, Phys. Rev. Appl. **15**, 024061 (2021).

[70] C. Whittle, E. D. Hall, S. Dwyer, N. Mavalvala, V. Sudhir, R. Abbott, A. Ananyeva, C. Austin, L. Barsotti, J. Betzwieser *et al.*, Approaching the motional ground state of a 10-kg object, Science **372**, 1333 (2021).

[71] B. D. Wood, S. Bose, and G. W. Morley, Spin dynamical decoupling for generating macroscopic superpositions of a free-falling nanodiamond, Phys. Rev. A **105**, 012824 (2022).

[72] B. Naydenov, F. Dolde, L. T. Hall, C. Shin, H. Fedder, L. C. L. Hollenberg, F. Jelezko, and J. Wrachtrup, Dynamical decoupling of a single-electron spin at room temperature, Phys. Rev. B **83**, 081201(R) (2011).

[73] J. Tisler, G. Balasubramanian, B. Naydenov, R. Kolesov, B. Grotz, R. Reuter, J.-P. Boudou, P. A. Curmi, M. Sennour, A. Thorel *et al.*, Fluorescence and spin properties of defects in single digit nanodiamonds, ACS Nano **3**, 1959 (2009).

[74] A. Laraoui, J. S. Hodges, and C. A. Meriles, Nitrogen-vacancy-assisted magnetometry of paramagnetic centers in an individual diamond nanocrystal, Nano Lett. **12**, 3477 (2012).

[75] B. D. Wood, G. A. Stimpson, J. E. March, Y. N. D. Lekhai, C. J. Stephen, B. L. Green, A. C. Frangeskou, L. Gins, S. Mandal, O. A. Williams *et al.*, Long spin coherence times of nitrogen

vacancy centers in milled nanodiamonds, Phys. Rev. B **105**, 205401 (2022).

[76] H. S. Knowles, D. M. Kara, and M. Atatüre, Observing bulk diamond spin coherence in high-purity nanodiamonds, Nat. Mater. **13**, 21 (2014).

[77] A. A. Wood, R. M. Goldblatt, R. E. Scholten, and A. M. Martin, Quantum control of nuclear-spin qubits in a rapidly rotating diamond, Phys. Rev. Res. **3**, 043174 (2021).

[78] A. Cabello, Experimentally Testable State-Independent Quantum Contextuality, Phys. Rev. Lett. **101**, 210401 (2008).

[79] G. Feinberg and J. Sucher, General theory of the van der waals interaction: A model-independent approach, Phys. Rev. A **2**, 2395 (1970).

[80] H. B. Casimir and D. Polder, The influence of retardation on the London-van der Waals forces, Phys. Rev. **73**, 360 (1948).

[81] J. S. Pedernales, G. W. Morley, and M. B. Plenio, Motional Dynamical Decoupling for Interferometry with Macroscopic Particles, Phys. Rev. Lett. **125**, 023602 (2020).

[82] H.-Y. Kim, J. O. Sofo, D. Velegol, M. W. Cole, and G. Mukhopadhyay, Static polarizabilities of dielectric nanoclusters, Phys. Rev. A **72**, 053201 (2005).

[83] M. Toroš, T. W. van de Kamp, R. J. Marshman, M. Kim, A. Mazumdar, and S. Bose, Relative acceleration noise mitigation for nanocrystal matter-wave interferometry: Applications to en-

tangling masses via quantum gravity, Phys. Rev. Res. **3**, 023178 (2021).

[84] H. Chevalier, A. J. Paige, and M. S. Kim, Witnessing the nonclassical nature of gravity in the presence of unknown interactions, Phys. Rev. A **102**, 022428 (2020).

[85] T. Kiss, P. Adam, and J. Janszky, Time-evolution of a harmonic oscillator: jumps between two frequencies, Phys. Lett. A **192**, 311 (1994).

[86] G. Afek, F. Monteiro, B. Siegel, J. Wang, S. Dickson, J. Recoaro, M. Watts, and D. C. Moore, Control and measurement of electric dipole moments in levitated optomechanics, Phys. Rev. A **104**, 053512 (2021).

[87] A. D. Rider, D. C. Moore, C. P. Blakemore, M. Louis, M. Lu, and G. Gratta, Search for Screened Interactions Associated with Dark Energy Below the 100 μm length scale, Phys. Rev. Lett. **117**, 101101 (2016).

[88] A. C. Frangeskou, A. Rahman, L. Gines, S. Mandal, O. A. Williams, P. F. Barker, and G. Morley, Pure nanodiamonds for levitated optomechanics in vacuum, New J. Phys. **20**, 043016 (2018).

[89] S. Sadana, B. C. Sanders, and U. Sinha, Double-slit interferometry as a lossy beam splitter, New J. Phys. **21**, 113022 (2019).

[90] C. Flühmann, T. L. Nguyen, M. Marinelli, V. Negnevitsky, K. Mehta, and J. Home, Encoding a qubit in a trapped-ion mechanical oscillator, Nature (London) **566**, 513 (2019).